

# First-Principles Dynamical Coherent-Potential Approximation Approach to the Ferromagnetism of Fe, Co, and Ni

Yoshiro KAKEHASHI\* and M. Atiqur R. PATOARY

*Department of Physics and Earth Sciences, Faculty of Science, University of the Ryukyus,  
1 Senbaru, Nishihara, Okinawa, 903-0213, Japan*

Magnetic properties of Fe, Co, and Ni at finite temperatures have been investigated on the basis of the first-principles dynamical CPA (Coherent Potential Approximation) combined with the LDA (Local Density Approximation) +  $U$  Hamiltonian in the Tight-Binding Linear Muffintin Orbital (TB-LMTO) representation. The Hamiltonian includes the transverse spin fluctuation terms. Numerical calculations have been performed within the harmonic approximation with 4th-order dynamical corrections. Calculated single-particle densities of states in the ferromagnetic state indicate that the dynamical effects reduce the exchange splitting, suppress the band width of the quasi-particle state, and causes incoherent excitations corresponding the 6 eV satellites. Results of the magnetization vs temperature curves, paramagnetic spin susceptibilities, and the amplitudes of local moments are presented. Calculated Curie temperatures ( $T_C$ ) are reported to be 1930K for Fe, 2550K for Co, and 620K for Ni;  $T_C$  for Fe and Co are overestimated by a factor of 1.8, while  $T_C$  in Ni agrees with the experimental result. Effective Bohr magneton numbers calculated from the inverse susceptibilities are  $3.0 \mu_B$  (Fe),  $3.0 \mu_B$  (Co), and  $1.6 \mu_B$  (Ni), being in agreement with the experimental ones. Overestimate of  $T_C$  in Fe and Co is attributed to the neglects of the higher-order dynamical effects as well as the magnetic short range order.

**KEYWORDS:** dynamical CPA, metallic magnetism, iron, cobalt, nickel, Curie temperature, effective Bohr magneton number, excitation spectra

## 1. Introduction

The 3d transition metals, Fe, Co, and Ni are well-known to show the ferromagnetism with rather high Curie temperatures 1040 K, 1388 K, and 630 K.<sup>1-3)</sup> Magnetic properties of these materials are characterized by the itinerant as well as local-moment behaviors.<sup>4)</sup> According to the angle resolved photoemission spectroscopy,<sup>5,6)</sup> quasiparticle  $d$  bands with the Fermi surface are observed in these transition metals, and the noninteger ground-state magnetizations per atom in unit of the Bohr magneton number ( $\mu_B$ ) are found;<sup>7,8)</sup>  $2.2 \mu_B$  (Fe),  $1.72 \mu_B$  (Co), and  $0.62 \mu_B$  (Ni). These results indicate that the 3d electrons are itinerant. On the other hand, the Curie-Weiss law in the susceptibility with atomic effective Bohr magneton number,<sup>9)</sup> the Brillouin-like magnetization vs temperature curve,<sup>10-12)</sup> and a large peak of the specific heat at the Curie temperature ( $T_C$ )<sup>13-15)</sup> are well explained by a simple local-moment model.

The itinerant vs local-moment behavior in 3d transition metals has been a long-standing problem in the metallic magnetism. The Stoner model combined with the first-principles band theory yields the Curie temperatures being much higher than the experimental ones; 6000K for Fe and 3000K for Ni,<sup>16,17)</sup> and does not explain the Curie-Weiss law. The theory has been much improved by taking into account spin fluctuations. Hubbard<sup>18)</sup> and Hasegawa<sup>19)</sup> proposed a single-site spin fluctuation theory (SSF) on the basis of the functional integral method.<sup>20-23)</sup> The theory interpolates between the weak and strong Coulomb interaction limits and ex-

plained qualitatively the magnetization vs temperature curve as well as the Curie-Weiss law on the basis of the band model. The theory however is based on the high-temperature approximation, *i.e.*, the static approximation which neglects the time dependence of the field variables. Therefore the SSF reduces to the Hartree-Fock approximation at the ground state, and thus does not take into account electron correlations as found in the ground state theories.<sup>24-29)</sup>

Takehashi and Fulde<sup>30)</sup> proposed a variational theory which takes into account the electron correlations at the ground state and reduces to the SSF at high-temperatures. They found that the reduction of the Curie temperature by a factor of two in the case of Fe. Hasegawa<sup>31)</sup> developed the same type of theory on the basis of the Slave-Boson functional integral approach. Although these theories include the ground-state electron correlations within the Gutzwiller-type approximation,<sup>24-26,32)</sup> systematic improvement of thermodynamics is not easy in these approaches. We therefore proposed a theory called the dynamical coherent potential approximation (CPA)<sup>33)</sup> which completely takes into account the dynamical charge and spin fluctuations within the single-site approximations, and clarified numerically the basic aspects of the theory with use of a Monte-Carlo technique.

In order to simplify numerical calculations, we proposed in the next paper,<sup>34)</sup> which we refer to I, more analytic theory of the dynamical CPA using the harmonic approximation, and verified on the basis of the Hubbard model that the dynamical effects reduce the Curie temperatures, cause the band narrowing for quasi-particle states, and create the '6 eV' satellite peak in ex-

\*E-mail address: yok@sci.u-ryukyu.ac.jp, to be published in J. Phys. Soc. Jpn.

citation spectra. In our recent paper,<sup>35)</sup> which we refer to II in the following, we proposed the first-principles dynamical CPA. The theory combines the dynamical CPA with the Local Density Approximation (LDA) + U scheme<sup>36)</sup> in the tight-binding linear muffin-tin orbital (TB-LMTO)<sup>37)</sup> representation. We investigated the dynamical effects on the magnetic properties of Fe and Ni within the 2nd-order dynamical corrections. Quite recently, we have improved the first-principles dynamical CPA taking into account the higher-order corrections,<sup>38)</sup> and clarified the systematic change of excitation spectra in 3d transition metal series.

In this paper, we present numerical results of calculations for the magnetic properties of Fe, Co, and Ni which are obtained by the 4th-order first-principles dynamical CPA. We investigate the dynamical effects on various quantities, and clarify the quantitative aspects of the first-principles dynamical CPA on the magnetic properties.

As we have proven in our previous papers,<sup>4,39)</sup> the dynamical CPA is equivalent to the many-body CPA<sup>40)</sup> in disordered alloys, the dynamical mean-field theory (DMFT)<sup>41–45)</sup> in the metal-insulator transition, and the projection operator CPA<sup>46)</sup> in excitation problem in solids. The first-principles DMFT calculations for Fe and Ni at the ground state have been performed by Miura and Fujiwara<sup>47)</sup> within the iterative perturbation method. The finite-temperature DMFT calculations for Fe and Ni have been performed by using the Hamiltonian without transverse spin fluctuations.<sup>48)</sup> We present here the finite-temperature results for the Hamiltonian with transverse spin fluctuations including the results for Co.

In the following section, we outline the first-principles dynamical CPA starting from the TB-LMTO type of Hamiltonian with intraatomic Coulomb interactions, and elucidate how to take into account the higher-order dynamical corrections using the asymptotic approximation. In §3, we present the numerical results of the densities of states, effective potentials, magnetization vs temperature curves, paramagnetic susceptibilities, and the amplitudes of local moments as a function of temperature. We will discuss on the dynamical effects on these physical quantities and quantitative aspects of the theory. Especially, we will demonstrate that high-temperature physical quantities such as the effective Bohr magneton number are qualitatively described by the present theory. We summarize our results in the last section §4, and discuss remaining problems.

## 2. First-principles TB-LMTO dynamical CPA

We adopt in the present paper the TB-LMTO Hamiltonian combined with a LDA+U Coulomb interactions as follows.<sup>35)</sup>

$$H = H_0 + H_1, \quad (1)$$

$$H_0 = \sum_{iL\sigma} (\epsilon_L^0 - \mu) \hat{n}_{iL\sigma} + \sum_{iLjL'\sigma} t_{iLjL'} a_{iL\sigma}^\dagger a_{jL'\sigma}, \quad (2)$$

$$H_1 = \sum_i \left[ \sum_m U_0 \hat{n}_{ilm\uparrow} \hat{n}_{ilm\downarrow} + \sum_{m>m'} (U_1 - \frac{1}{2}J) \times \hat{n}_{ilm} \hat{n}_{ilm'} - \sum_{m>m'} J \hat{s}_{ilm} \cdot \hat{s}_{ilm'} \right]. \quad (3)$$

Here we assumed a transition metal with an atom per unit cell.  $\epsilon_L^0$  is an atomic level on site  $i$  and orbital  $L$ ,  $\mu$  is the chemical potential,  $t_{iLjL'}$  is a transfer integral between orbitals  $iL$  and  $jL'$ .  $L = (l, m)$  denotes  $s$ ,  $p$ , and  $d$  orbitals.  $a_{iL\sigma}^\dagger$  ( $a_{iL\sigma}$ ) is the creation (annihilation) operator for an electron with orbital  $L$  and spin  $\sigma$  on site  $i$ , and  $\hat{n}_{iL\sigma} = a_{iL\sigma}^\dagger a_{iL\sigma}$  is a charge density operator for electrons with orbital  $L$  and spin  $\sigma$  on site  $i$ .

The Coulomb interaction term  $H_1$  consists of the on-site interactions between  $d$  electrons ( $l = 2$ ).  $U_0$  ( $U_1$ ) and  $J$  denote the intra-orbital (inter-orbital) Coulomb and exchange interactions, respectively.  $\hat{n}_{ilm}$  ( $\hat{s}_{ilm}$ ) with  $l = 2$  is the charge (spin) density operator for  $d$  electrons on site  $i$  and orbital  $m$ . Note that the atomic level  $\epsilon_L^0$  in  $H_0$  is not identical with the LDA atomic level  $\epsilon_L$ ;  $\epsilon_L^0 = \epsilon_L - \partial E_{\text{LDA}}^U / \partial n_{iL\sigma}$ . Here  $n_{iL\sigma}$  is the charge density at the ground state,  $E_{\text{LDA}}^U$  is a LDA functional to the intraatomic Coulomb interactions.<sup>36,49)</sup>

In the dynamical CPA, we transform in the free energy the interacting Hamiltonian  $H_1$  into a one-body Hamiltonian with dynamical potential  $v$  for time-dependent random charge and exchange fields, using the functional integral method.<sup>23,35)</sup> Introducing a site-diagonal uniform medium, *i.e.*, a coherent potential  $\Sigma$  into the potential part, we expand the correction  $v - \Sigma$  with respect to sites. The zeroth term in the expansion is the free energy for a uniform medium,  $\tilde{\mathcal{F}}[\Sigma]$ . The next term is an impurity contribution to the free energy. The dynamical CPA neglects the higher-order terms associated with inter-site correlations. The free energy per atom is then given by<sup>34,35)</sup>

$$\mathcal{F}_{\text{CPA}} = \tilde{\mathcal{F}}[\Sigma] - \beta^{-1} \ln \int \left[ \prod_{\alpha} \sqrt{\frac{\beta \tilde{J}_{\alpha}}{4\pi}} d\xi_{\alpha} \right] e^{-\beta E_{\text{eff}}(\boldsymbol{\xi})}. \quad (4)$$

Here  $\beta$  is the inverse temperature,  $\tilde{J}_x = \tilde{J}_y = \tilde{J}_{\perp} = [1 - 1/(2l+1)]J$ ,  $\tilde{J}_z = U_0/(2l+1) + \tilde{J}_{\perp}$ , and  $\boldsymbol{\xi} = (\xi_x, \xi_y, \xi_z)$  is a static field variable on a site.

The effective potential  $E_{\text{eff}}(\boldsymbol{\xi})$  in eq. (4) consists of the static contribution  $E_{\text{st}}(\boldsymbol{\xi})$  and the dynamical correction term  $E_{\text{dyn}}(\boldsymbol{\xi})$  as follows.

$$E_{\text{eff}}(\boldsymbol{\xi}) = E_{\text{st}}(\boldsymbol{\xi}) + E_{\text{dyn}}(\boldsymbol{\xi}). \quad (5)$$

The former is given as

$$E_{\text{st}}(\boldsymbol{\xi}) = -\frac{1}{\beta} \sum_{mn} \ln \left[ (1 - \delta v_{L\uparrow}(0) F_{L\uparrow}(i\omega_n)) (1 - \delta v_{L\downarrow}(0) \times F_{L\downarrow}(i\omega_n)) - \frac{1}{4} \tilde{J}_{\perp}^2 \xi_{\perp}^2 F_{L\uparrow}(i\omega_n) F_{L\downarrow}(i\omega_n) \right] + \frac{1}{4} \left[ - (U_0 - 2U_1 + J) \sum_m \tilde{n}_L(\boldsymbol{\xi})^2 \right]$$

$$-(2U_1 - J)\tilde{n}_l(\boldsymbol{\xi})^2 + \tilde{J}_\perp^2 \xi_\perp^2 + \tilde{J}_z^2 \xi_z^2. \quad (6)$$

Here  $\delta v_{L\sigma}(0) = v_{L\sigma}(0) - \Sigma_{L\sigma}(i\omega_n)$ , and  $\xi_\perp^2 = \xi_x^2 + \xi_y^2$ .  $v_{L\sigma}(0)$  is a static potential given by  $v_{L\sigma}(0) = [(U_0 - 2U_1 + J)\tilde{n}_{lm}(\boldsymbol{\xi}) + (2U_1 - J)\tilde{n}_l(\boldsymbol{\xi})]/2 - \tilde{J}_z \xi_z \sigma/2$ ,  $\Sigma_{L\sigma}(i\omega_n)$  is the coherent potential in Matsubara frequency representation, and  $\omega_n = (2n + 1)\pi/\beta$ . The electron number  $\tilde{n}_L(\boldsymbol{\xi})$  for a given  $\boldsymbol{\xi}$  is expressed by means of an impurity Green function as

$$\tilde{n}_L(\boldsymbol{\xi}) = \frac{1}{\beta} \sum_{n\sigma} G_{L\sigma}(\boldsymbol{\xi}, i\omega_n), \quad (7)$$

and  $\tilde{n}_l(\boldsymbol{\xi}) = \sum_m \tilde{n}_L(\boldsymbol{\xi})$ . The impurity Green function  $G_{L\sigma}(\boldsymbol{\xi}, i\omega_n)$  has to be determined self-consistently. The explicit expression will be given later (see eq. (32)).

The coherent Green function  $F_{L\sigma}(i\omega_n)$  in eq. (6) is defined by

$$F_{L\sigma}(i\omega_n) = [(i\omega_n - \mathbf{H}_0 - \boldsymbol{\Sigma}(i\omega_n))^{-1}]_{iL\sigma iL\sigma}. \quad (8)$$

Here  $(\mathbf{H}_0)_{iL\sigma jL'\sigma}$  is the one-electron Hamiltonian matrix for the noninteracting Hamiltonian  $H_0$ , and  $(\boldsymbol{\Sigma}(i\omega_n))_{iL\sigma jL'\sigma} = \Sigma_{L\sigma}(i\omega_n)\delta_{ij}\delta_{LL'}$ .

The dynamical potential  $E_{\text{dyn}}(\boldsymbol{\xi})$  in eq. (5) has been obtained within the harmonic approximation.<sup>34, 35, 50, 51</sup> It is based on an expansion of  $E_{\text{dyn}}(\boldsymbol{\xi})$  with respect to the frequency mode of the dynamical potential  $v_{L\sigma\sigma'}(i\omega_\nu)$ , where  $\omega_\nu = 2\nu\pi/\beta$ . The harmonic approximation is the neglect of the mode-mode coupling terms in the expansion. We have then

$$E_{\text{dyn}}(\boldsymbol{\xi}) = -\beta^{-1} \ln \left[ 1 + \sum_{\nu=1}^{\infty} (\overline{D}_\nu - 1) \right]. \quad (9)$$

Here the determinant  $D_\nu$  is a contribution from a dynamical potential  $v_{L\sigma\sigma'}(i\omega_\nu)$  with frequency  $\omega_\nu$ , and the upper bar denotes a Gaussian average with respect to the dynamical charge and exchange field variables,  $\zeta_m(i\omega_n)$  and  $\xi_{m\alpha}(i\omega_n)$  ( $\alpha = x, y, z$ ).

The determinant  $D_\nu$  is expressed as<sup>35</sup>

$$D_\nu = \prod_{k=0}^{\nu-1} \left[ \prod_{m=1}^{2l+1} D_\nu(k, m) \right], \quad (10)$$

$$D_\nu(k, m) = \begin{vmatrix} \ddots & & & & & \\ & 1 & & 1 & & 0 \\ a_{-\nu+k}(\nu, m) & 1 & & 1 & & \\ & a_k(\nu, m) & 1 & & 1 & \\ & & a_{\nu+k}(\nu, m) & 1 & & 1 \\ 0 & & & a_{2\nu+k}(\nu, m) & & \\ & & & & \ddots & \end{vmatrix}. \quad (11)$$

Note that 1 in the above determinant denotes the  $2 \times 2$  unit matrix,  $a_n(\nu, m)$  is a  $2 \times 2$  matrix defined by

$$a_n(\nu, m)_{\sigma\sigma'} = \sum_{\sigma''\sigma'''\sigma''''} v_{L\sigma\sigma''}(i\omega_\nu) \tilde{g}_{L\sigma''\sigma'''}(i\omega_n - i\omega_\nu) \times v_{L\sigma'''\sigma''''}(-i\omega_\nu) \tilde{g}_{L\sigma''''\sigma'}(i\omega_n), \quad (12)$$

$$v_{L\sigma\sigma'}(i\omega_\nu) = -\frac{1}{2} \sum_{m'} iA_{mm'} \zeta_{m'}(i\omega_\nu) \delta_{l2} \delta_{\sigma\sigma'}$$

$$-\frac{1}{2} \sum_{\alpha} \sum_{m'} B_{mm'}^{\alpha} \xi_{m'\alpha}(i\omega_\nu) \delta_{l2} (\sigma_{\alpha})_{\sigma\sigma'}, \quad (13)$$

$$\tilde{g}_{L\sigma\sigma'}(i\omega_n) = [(F_L(i\omega_n)^{-1} - \delta v_0)^{-1}]_{\sigma\sigma'}. \quad (14)$$

Here  $\sigma_{\alpha}$  ( $\alpha = x, y, z$ ) are the Pauli spin matrices.  $A_{mm'} = U_0 \delta_{mm'} + (2U_1 - J)(1 - \delta_{mm'})$ ,  $B_{mm'}^{\alpha} = J(1 - \delta_{mm'})$  ( $\alpha = x, y$ ), and  $B_{mm'}^z = U_0 \delta_{mm'} + J(1 - \delta_{mm'})$ .  $\tilde{g}_{L\sigma\sigma'}(i\omega_n)$  is the impurity Green function in the static approximation,  $(F_L(i\omega_n))_{\sigma\sigma'} = F_{L\sigma}(i\omega_n) \delta_{\sigma\sigma'}$ , and  $\delta v_0$  is defined by  $(\delta v_0)_{\sigma\sigma'} = v_{L\sigma\sigma'}(0) - \Sigma_{L\sigma}(i\omega_n) \delta_{\sigma\sigma'}$ .

The determinant  $D_\nu(k, m)$  is expanded with respect to the dynamical potential as follows.

$$D_\nu(k, m) = 1 + D_\nu^{(1)}(k, m) + D_\nu^{(2)}(k, m) + \cdots, \quad (15)$$

$$D_\nu^{(n)}(k, m) = \sum_{\alpha_1 \gamma_1 \cdots \alpha_n \gamma_n} v_{\alpha_1}(\nu, m) v_{\gamma_1}(-\nu, m) \cdots \times v_{\alpha_n}(\nu, m) v_{\gamma_n}(-\nu, m) \hat{D}_{\{\alpha\gamma\}}^{(n)}(\nu, k, m). \quad (16)$$

Here the subscripts  $\alpha_i$  and  $\gamma_i$  take 4 values 0,  $x$ ,  $y$ , and  $z$ , and

$$v_0(\nu, m) = -\frac{1}{2} i \sum_{m'} A_{mm'} \zeta_{m'}(i\omega_\nu) \delta_{l2}, \quad (17)$$

$$v_{\alpha}(\nu, m) = -\frac{1}{2} \sum_{m'} B_{mm'}^{\alpha} \xi_{m'\alpha}(i\omega_\nu) \delta_{l2}, \quad (\alpha = x, y, z). \quad (18)$$

Note that the subscript  $\{\alpha\gamma\}$  of  $\hat{D}_{\{\alpha\gamma\}}^{(n)}(\nu, k, m)$  in eq. (16) denotes a set of  $(\alpha_1 \gamma_1, \cdots, \alpha_n \gamma_n)$ .

Substituting eq. (15) into eq. (10) and taking the Gaussian average, we reach

$$E_{\text{dyn}}(\boldsymbol{\xi}) = -\beta^{-1} \ln \left( 1 + \sum_{n=1}^{\infty} \sum_{\nu=1}^{\infty} \overline{D}_\nu^{(n)} \right), \quad (19)$$

and

$$\overline{D}_\nu^{(n)} = \frac{1}{(2\beta)^n} \sum_{\sum_{km} l(k, m) = n} \sum_{\{\alpha_j(k, m)\}} \sum_P \prod_{m=1}^{2l+1} \prod_{k=0}^{\nu-1} \times \left[ \left( \prod_{j=1}^{l(k, m)} C_{mm_p}^{\alpha_j(k, m)} \right) \hat{D}_{\{\alpha_{p-1}\}}^{(l(k, m))}(\nu, k, m) \right]. \quad (20)$$

Here each element of  $\{l(k, m)\}$  ( $k = 0, \cdots, \nu - 1, m = 1, \cdots, 2l + 1$ ) has a value of zero or positive integer.  $\alpha_j(k, m)$  takes one of 4 cases 0,  $x$ ,  $y$ , and  $z$ .  $j$  denotes the  $j$ -th member of the  $(k, m)$  block with  $l(k, m)$  elements.  $P$  denotes a permutation of a set  $\{(j, k, m)\}$ ;  $P\{(j, k, m)\} = \{(j_p, k_p, m_p)\}$ .  $\alpha_{p-1}$  means a rearrangement of  $\{\alpha_j(k, m)\}$  according to the inverse permutation  $P^{-1}$ . The coefficient  $C_{mm'}^{\alpha}$  in eq. (20) is a Coulomb interaction defined by

$$C_{mm'}^{\alpha} = \begin{cases} -A_{mm'} & (\alpha = 0) \\ B_{mm'}^{\alpha} & (\alpha = x, y, z) \end{cases}. \quad (21)$$

The frequency dependent factors  $\hat{D}_{\{\alpha\gamma\}}^{(n)}(\nu, k, m)$  in eq. (20) consist of a linear combination of  $2n$  products of the static Green functions. Their first few terms have been given in Appendix A of our paper II.<sup>35)</sup>

In the calculations of the higher-order dynamical corrections<sup>38)</sup>  $\hat{D}_{\{\alpha\gamma\}}^{(n)}(\nu, k, m)$ , we note that the coupling constants  $B_{mm'}^x = B_{mm'}^y = J(1 - \delta_{mm'})$  are much smaller than  $A_{mm'}$  and  $B_{mm'}^z$  because  $U_0$  and  $U_1 \gg J$ . Thus we neglect the transverse potentials,  $v_x(\nu, m)$  and  $v_y(\nu, m)$ . The approximation implies that  $a_n(\nu, m)_{\sigma-\sigma} = 0$ . The determinant  $D_\nu(k, m)$  in eq. (10) is then written by the products of the single-spin components as

$$D_\nu(k, m) = D_{\nu\uparrow}(k, m)D_{\nu\downarrow}(k, m). \quad (22)$$

Here  $D_{\nu\sigma}(k, m)$  is defined by eq. (11) in which the  $2 \times 2$  unit matrices have been replaced by 1 (*i.e.*,  $1 \times 1$  unit matrices), and the  $2 \times 2$  matrices  $a_n(\nu, m)$  have been replaced by the  $1 \times 1$  matrices  $a_n(\nu, m)_{\sigma\sigma}$ . The latter is given by

$$a_n(\nu, m)_{\sigma\sigma} = \sum_{\alpha, \gamma}^{0, z} v_\alpha(\nu, m) v_\gamma(-\nu, m) \hat{h}_{\alpha\gamma\sigma} e_{n\sigma}(\nu, m), \quad (23)$$

$$e_{n\sigma}(\nu, m) = \tilde{g}_{L\sigma}(n - \nu) \tilde{g}_{L\sigma}(n). \quad (24)$$

Here  $\hat{h}_{\alpha\gamma\sigma} = \delta_{\alpha\gamma} + \sigma(1 - \delta_{\alpha\gamma})$ , and we used a notation  $\tilde{g}_{L\sigma}(n) = \tilde{g}_{L\sigma\sigma}(i\omega_n)$  for simplicity.

In order to reduce these summations, we make use of an asymptotic approximation.<sup>34, 38)</sup>

$$e_{n\sigma}(\nu, m) \sim \bar{q}_\nu (\tilde{g}_{L\sigma}(n - \nu) - \tilde{g}_{L\sigma}(n)), \quad (25)$$

where  $\bar{q}_\nu = \beta/2\pi\nu i$ . The approximation is justified in the high-frequency limit where  $\tilde{g}_{L\sigma}(n)$  written as

$$\tilde{g}_{L\sigma}(n) = \frac{1}{i\omega_n - \epsilon_L^0 + \mu - v_{L\sigma}(0)} + O\left(\frac{1}{(i\omega_n)^3}\right). \quad (26)$$

In the asymptotic approximation, we obtain

$$\begin{aligned} \hat{D}_{\{\alpha\gamma\}}^{(n)}(\nu, k, m) &= \sum_{l=0}^n \hat{D}_{\{\alpha_1\gamma_1 \dots \alpha_l\gamma_l\}}^{(l)}(\nu, k, m) \\ &\quad \times \hat{D}_{\{\alpha_{l+1}\gamma_{l+1} \dots \alpha_n\gamma_n\}}^{(n-l)}(\nu, k, m). \end{aligned} \quad (27)$$

Here we wrote the subscript at the r.h.s. explicitly to avoid confusion. Note that the values of  $\alpha_i$  and  $\gamma_i$  are limited to 0 or  $z$  in the present approximation. The spin-dependent quantities are given by<sup>38)</sup>

$$\hat{D}_{\{\alpha\gamma\}\sigma}^{(l)}(\nu, k, m) = \Lambda_\sigma^{(l)}(\{\alpha\gamma\}) \frac{\bar{q}_\nu^i}{l!} B_\sigma^{(l)}(\nu, k, m), \quad (28)$$

$$\Lambda_\sigma^{(l)}(\{\alpha\gamma\}) = \begin{cases} 1 & (\sigma = \uparrow) \\ (-1)^{l-n_l(\{\alpha\gamma\})} & (\sigma = \downarrow) \end{cases}, \quad (29)$$

$$\begin{aligned} B_\sigma^{(l)}(\nu, k, m) &= \left[ \prod_{j=0}^{l-1} \tilde{g}_{L\sigma}(j\nu + k) \right] \\ &\quad + \sum_{i=0}^{l-1} \frac{(-)^{l-i} l!}{i! (l-i)!} \left[ \prod_{j=-(l-i)}^{i-1} \tilde{g}_{L\sigma}(j\nu + k) \right] \end{aligned}$$

$$\times \left[ 1 + \frac{l-i}{\bar{q}_\nu} \tilde{g}_{L\sigma}(i\nu + k) \right]. \quad (30)$$

Here  $\hat{D}_{\{\alpha\gamma\}\sigma}^{(0)}(\nu, k, m) = 1$ .  $n_l(\{\alpha\gamma\})$  is the number of  $\{\alpha_i\gamma_i\}$  pairs such that  $\alpha_i = \gamma_i$  among the  $l$  pairs. When there is no orbital degeneracy, eq. (30) reduces to the result of the zeroth asymptotic approximation in our paper I.<sup>34)</sup>

In the actual applications we make use of the exact form up to a certain order of expansion in  $\bar{D}_\nu^{(m)}$ , and for higher order terms we adopt an approximate form (27). In this way, we can take into account dynamical corrections systematically starting from both sides, the weak interaction limit and the high-temperature one.

The coherent potential can be determined by the stationary condition  $\delta\mathcal{F}_{\text{CPA}}/\delta\Sigma = 0$ . This yields the CPA equation as<sup>35)</sup>

$$\langle G_{L\sigma}(\xi, i\omega_n) \rangle = F_{L\sigma}(i\omega_n). \quad (31)$$

Here  $\langle \rangle$  at the l.h.s. (left-hand-side) is a classical average taken with respect to the effective potential  $E_{\text{eff}}(\xi)$ . The impurity Green function is given by

$$G_{L\sigma}(\xi, i\omega_l) = \tilde{g}_{L\sigma\sigma}(i\omega_l) + \frac{\sum_n \sum_\nu \frac{\delta \bar{D}_\nu^{(n)}}{\kappa_{L\sigma}(i\omega_l) \delta \Sigma_{L\sigma}(i\omega_l)}}{1 + \sum_n \sum_\nu \bar{D}_\nu^{(n)}}. \quad (32)$$

Note that the first term at the r.h.s. (right-hand-side) is the impurity Green function in the static approximation, which is given by eq. (14). The second term is the dynamical corrections, and  $\kappa_{L\sigma}(i\omega_l) = 1 - F_{L\sigma}(i\omega_l)^{-2} \delta F_{L\sigma}(i\omega_l) / \delta \Sigma_{L\sigma}(i\omega_l)$ .

Solving the CPA equation (31) self-consistently, we obtain the effective medium. The electron number on each orbital  $L$  is then calculated from

$$\langle \hat{n}_L \rangle = \frac{1}{\beta} \sum_{n\sigma} F_{L\sigma}(i\omega_n). \quad (33)$$

The chemical potential  $\mu$  is determined from the condition  $n_e = \sum_L \langle \hat{n}_L \rangle$ . Here  $n_e$  denotes the conduction electron number per atom. The magnetic moment is given by

$$\langle \hat{m}_L^z \rangle = \frac{1}{\beta} \sum_{n\sigma} \sigma F_{L\sigma}(i\omega_n). \quad (34)$$

In particular, the  $l = 2$  component of magnetic moment is expressed as

$$\langle \hat{m}_l \rangle = \langle \xi \rangle. \quad (35)$$

The above relation implies that the effective potential  $E_{\text{eff}}(\xi)$  is a potential energy for a local magnetic moment  $\xi$ .

In the numerical calculations, we took into account the dynamical corrections up to the second order ( $n \leq 2$ ) exactly, and the higher-order terms up to the fourth order within the asymptotic approximation. Summation with respect to  $\nu$  in Eqs. (19) and (32) was taken up to  $\nu = 100$  for  $n = 1$  and 2, and up to  $\nu = 2$  for  $n = 3, 4$ .

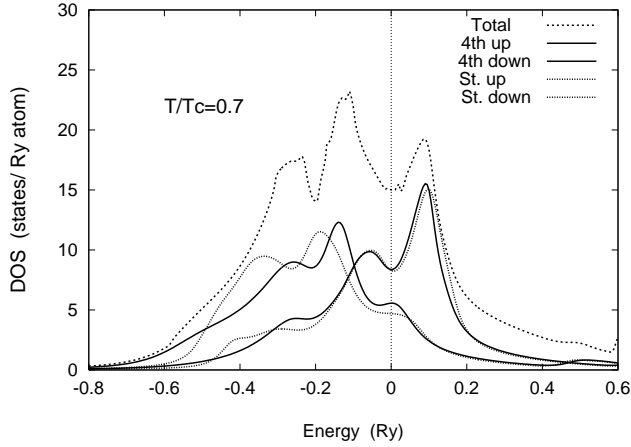


**Fig. 1.** Up and down  $d$  partial densities of states (DOS) of Fe in the static approximation (dotted curves) and in the 4th-order dynamical CPA (solid curves). The total DOS in the 4th-order dynamical CPA is shown by dashed curve.

When we solve the CPA equation (31), we adopted a decoupling approximation to the thermal average of impurity Green function<sup>52)</sup> for simplicity, *i.e.*,

$$\begin{aligned} & \langle G_{L\sigma}(\xi_z, \xi_{\perp}^2, i\omega_n) \rangle \\ &= \sum_{q=\pm} \frac{1}{2} \left( 1 + q \frac{\langle \xi_z \rangle}{\sqrt{\langle \xi_z^2 \rangle}} \right) G_{L\sigma}(q\sqrt{\langle \xi_z^2 \rangle}, \xi_{\perp}^2, i\omega_n). \end{aligned} \quad (36)$$

Here we wrote the static exchange field  $\xi$  as  $(\xi_z, \xi_{\perp}^2)$  so that the decoupling approximation we made becomes clearer. The approximation is correct up to the second moment (*i.e.*,  $\langle \xi_{\alpha}^2 \rangle$ ) and allows us to describe the thermal spin fluctuations in a simpler way.

On the other hand, we adopted a diagonal approximation<sup>53)</sup> to the coherent Green function at the r.h.s. of eq. (31).

$$F_{L\sigma}(n) = \int \frac{\rho_L^{\text{LDA}}(\epsilon) d\epsilon}{i\omega_n - \epsilon - \Sigma_{L\sigma}(i\omega_n) - \Delta\epsilon_L}. \quad (37)$$

Here  $\rho_L^{\text{LDA}}(\epsilon)$  is the local density of states for the LDA band calculation, and  $\Delta\epsilon_L = (\epsilon_L - \epsilon_L^0)\delta_{l2}$ . The approximation partly takes into account the effects of hybridization between different  $l$  blocks in the nonmagnetic state, but neglects the effects via spin polarization.

The CPA equation (31) with use of the decoupling approximation (36) yields an approximate solution to the full CPA equation. For the calculations of the single-particle densities of states, one needs more accurate solution for the CPA self-consistent equation. For this purpose, we adopted the following average  $t$ -matrix approximation<sup>54,55)</sup> (ATA) after we solved eq. (31) with the decoupling approximation (36).

$$\Sigma_{L\sigma}^{\text{ATA}}(i\omega_n) = \Sigma_{L\sigma}(i\omega_n) + \frac{\langle G_{L\sigma}(\xi_z, \xi_{\perp}^2, i\omega_n) \rangle - F_{L\sigma}(i\omega_n)}{\langle G_{L\sigma}(\xi_z, \xi_{\perp}^2, i\omega_n) \rangle F_{L\sigma}(i\omega_n)}.$$

Here the coherent potential in the decoupling approximation is used at the r.h.s., but the full average  $\langle \rangle$  of the impurity Green function is taken. The ATA is a one-shot correction to the full CPA. The coherent poten-

tial  $\Sigma_{L\sigma}(z)$  on the real axis  $z = \omega + i\delta$  is then calculated by using the Padé numerical analytic continuation method.<sup>56)</sup> Here  $\delta$  is an infinitesimal positive number. The densities of states (DOS) as the single-particle excitations,  $\rho_{L\sigma}(\omega)$  are calculated from the relation,

$$\rho_{L\sigma}(\omega) = -\frac{1}{\pi} \text{Im} F_{L\sigma}(z). \quad (39)$$

### 3. Numerical results

In the numerical calculations, we adopted the lattice constants used by Andersen *et al.*,<sup>37)</sup> and performed the LDA calculations with use of the Barth-Hedin exchange-correlation potential to make the TB-LMTO Hamiltonian (2). For Fe and Ni, we adopted average Coulomb interaction parameters  $\bar{U}$  and the average exchange interactions  $\bar{J}$  used by Anisimov *et al.*,<sup>49)</sup> and for Co we adopted  $\bar{U}$  obtained by Bandyopadhyay *et al.*<sup>57)</sup> and  $\bar{J}$  obtained by the Hartree-Fock atomic calculations<sup>58)</sup>;  $\bar{U} = 0.169$  Ry and  $\bar{J} = 0.066$  Ry for bcc Fe,  $\bar{U} = 0.245$  Ry and  $\bar{J} = 0.069$  Ry for fcc Co, and  $\bar{U} = 0.221$  Ry and  $\bar{J} = 0.066$  Ry for fcc Ni. The intra-orbital Coulomb interaction  $U_0$ , inter-orbital Coulomb interaction  $U_1$ , and the exchange interaction energy parameter  $J$  were calculated from  $\bar{U}$  and  $\bar{J}$  as  $U_0 = \bar{U} + 8\bar{J}/5$ ,  $U_1 = \bar{U} - 2\bar{J}/5$ , and  $J = \bar{J}$ , using the relation  $U_0 = U_1 + 2J$ .

Figure 1 shows the calculated densities of states (DOS) in the ferromagnetic Fe. Thermal spin fluctuations in the static approximation broaden the band width for each spin band. The DOS with the 4th-order dynamical charge and spin fluctuations shifts the main peak towards the Fermi level and causes a small hump around  $\omega = -0.5$  Ry which corresponds to the ‘6 eV’ satellite as found in Ni at 6 eV below the Fermi level.<sup>59–63)</sup> The present calculations with dynamical effects yields the ground-state magnetization  $2.58 \mu_B$ , which is considerably larger than the experimental value  $2.22 \mu_B$ . The exchange splitting in the present calculations is therefore somewhat overestimated. When the exchange splitting is reduced, the main peak in the up spin band shifts up and the second peak of the down spin band shifts down, so that one expects that the main peak around  $\omega = -0.1$  Ry in the total DOS becomes sharper and shifts towards the Fermi level.

The effective potential in the dynamical CPA characterizes spin fluctuations of the system. Unlike the single band model,<sup>34)</sup> calculated potential for ferromagnetic Fe has the double minimum structure as shown in Fig. 2. This implies that Fe local magnetic moments show large thermal spin fluctuations which change magnetic moments in direction. In order to clarify the dynamical effects on the effective potential, we plotted the dynamical contribution  $E_{\text{dyn}}(\xi) = E_{\text{eff}}(\xi) - E_{\text{st}}(\xi)$  in Fig. 3. The dynamical potential of Fe has a saddle point at the origin;  $E_{\text{dyn}}(\xi)$  shows the minimum along the  $z$  axis, and the maximum along the  $x$  ( $y$ ) axis at the origin. It indicates that the dynamical effects reduce the longitudinal amplitude of magnetic moments and enhance the transverse spin fluctuations. These effects are enhanced with increasing temperatures.

The magnetization vs temperature curves of Fe in vari-

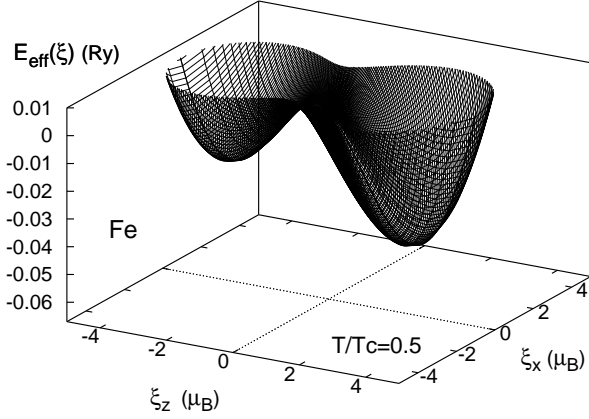


**Fig. 2.** Effective potential for Fe at the temperature  $T/T_C = 0.5$  on the  $\xi_x - \xi_z$  plane.

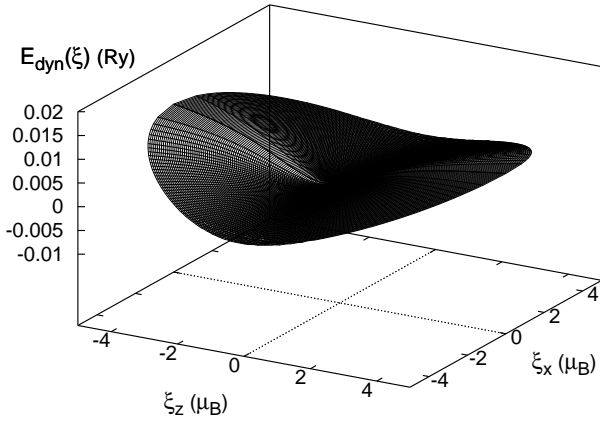


**Fig. 3.** Dynamical contribution to the effective potential for Fe at  $T/T_C = 0.5$ .

ous approximations are presented in Fig. 4. We obtained the Curie temperature  $T_C = 2070\text{K}$  in the static approximation. It is lower than that of the Hartree-Fock one ( $12200\text{K}$ ) by a factor of 6. The second-order dynamical corrections reduces  $T_C$  by  $50\text{K}$  as shown in Fig. 4. The 4th-order dynamical corrections further reduce  $T_C$  by  $90\text{K}$  as compared with the 2nd-order ones, and yield  $T_C = 1930\text{K}$ . The result is comparable to the value  $T = 1900\text{K}$  based on the DMFT without transverse spin fluctuations,<sup>48)</sup> but still overestimates  $T_C$  by a factor of 1.8 as compared with the experimental one ( $1040\text{K}$ ).<sup>1)</sup> Calculated inverse susceptibilities follows the Curie-Weiss law. We obtained the effective Bohr magneton number as  $3.1 \mu_B$  (static approximation),  $3.0 \mu_B$  (2nd-order dynamical CPA), and  $3.0 \mu_B$  (4th-order dynamical CPA), respectively. These values are in good agreement with the experimental value<sup>9)</sup>  $3.2 \mu_B$ . The amplitudes of local magnetic moments  $\langle m^2 \rangle^{1/2}$  show a

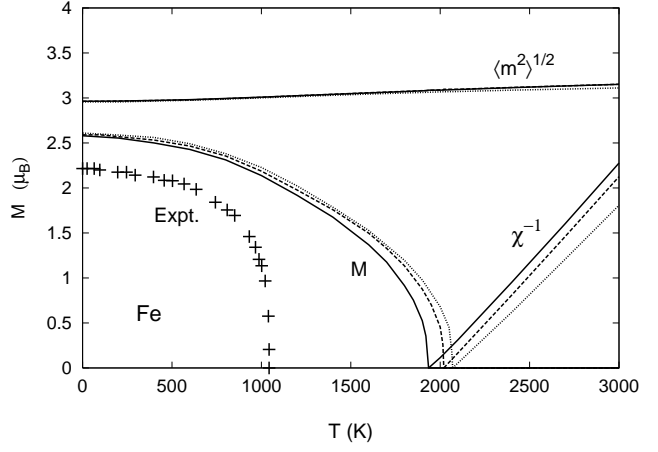


**Fig. 4.** Magnetization vs temperature curves ( $M - T$ ), inverse susceptibilities ( $\chi^{-1}$ ), and the amplitudes of local magnetic moments ( $\langle m^2 \rangle^{1/2}$ ) for Fe in the static approximation (dotted curves), the 2nd-order dynamical CPA (dashed curves), and the 4th-order dynamical CPA (solid curves), respectively. Experimental  $M - T$  curve<sup>10)</sup> is shown by + points.

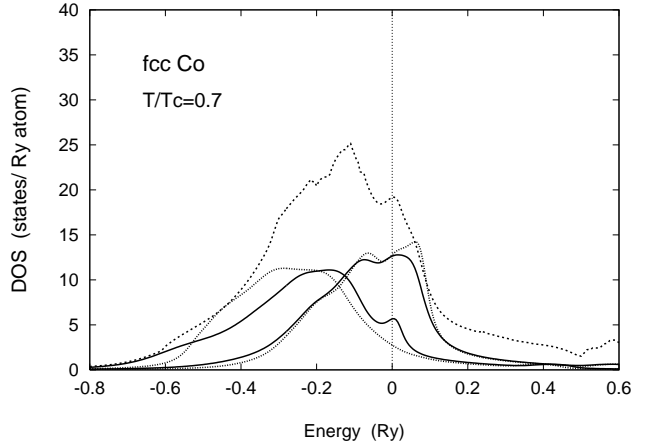


**Fig. 5.** Up and down  $d$  partial DOS of Co in the static approximation (dotted curves) and in the 4th-order dynamical CPA (solid curves). The total DOS in the 4th-order dynamical CPA is shown by dashed curve.

weak temperature dependence and take a value  $3.1 \mu_B$  at  $2000\text{K}$  irrespective of details of approximations as shown in Fig. 4. It should be noted that the calculated effective Bohr magneton number approximately equals to the amplitude of local moment; the Rhodes-Wohlfarth ratio is 1 in agreement with the experimental fact.

In the case of Co, the crystal structure changes from the hcp to the fcc with increasing temperature. We present here the results for the fcc Co. Figure 5 shows an example of calculated DOS in the ferromagnetic state. The  $d$  DOS are split into up and down parts. The  $d$  DOS in the static approximation are smoothed and are broadened due to thermal spin fluctuations. The dynamical effects reduce the exchange splitting and the band width of each spin component. More important difference between the static and dynamical cases is that the quasiparticle peaks appear at the Fermi level due to dynamical spin

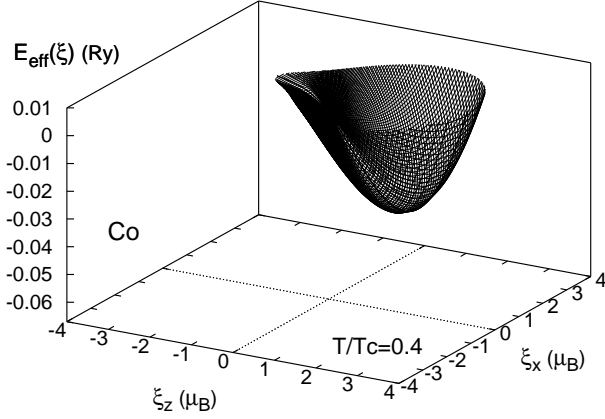


Fig. 6. Effective potential of Co at  $T/T_C = 0.4$ .

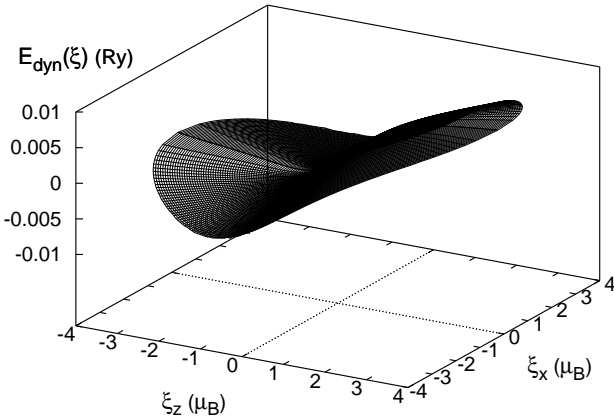


Fig. 7. Dynamical contribution to the effective potential in Co at  $T/T_C = 0.4$ .

and charge fluctuations. We also find a small hump at  $\omega = -0.55\text{Ry}$  in the up-spin DOS, which is caused by dynamical charge fluctuations.

We present in Fig. 6 the effective potential for fcc Co. The potential has a single minimum in the ferromagnetic state. With increasing temperature the flat part of the potential around the origin extends to the negative region of  $\xi_z$ , and the double minimum structure appears near and above  $T_C$ . The dynamical corrections to the effective potential show a butterfly structure in which the ala in the region  $\xi_z > 0$  is higher than that in  $\xi_z < 0$ , as shown in Fig. 7. It indicates that the dynamical effects act to reduce the magnetization and to enhance the transverse spin fluctuations.

Calculated magnetization vs temperature curves for fcc Co are shown in Fig. 8. We find the Curie temperature in the static approximation  $T_C = 3160\text{ K}$ . It is much lower than the Hartree-Fock one (12100 K). The 4th-order dynamical CPA reduces  $T_C$  by 610K, and yields

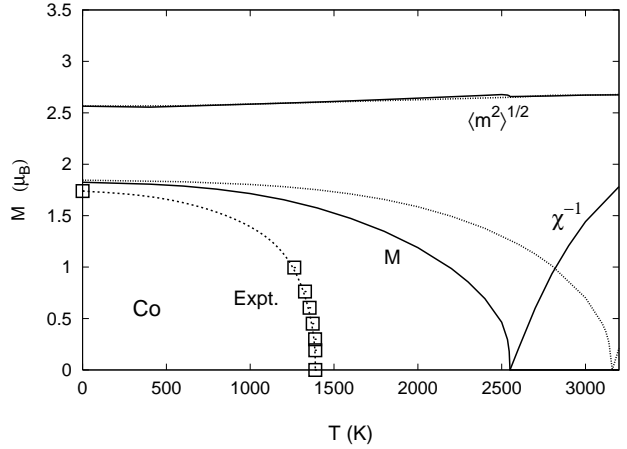


Fig. 8. Magnetization vs temperature curves ( $M - T$ ), inverse susceptibilities ( $\chi^{-1}$ ), and the amplitudes of local magnetic moments ( $\langle m^2 \rangle^{1/2}$ ) for Co in the static approximation (dotted curves) and the 4th-order dynamical CPA (solid curves), respectively. Experimental data of magnetizations<sup>11)</sup> for fcc Co are shown by open squares. Dashed line shows a guide for the eye to an experimental  $M - T$  curve.

$T_C = 2550\text{K}$ . The latter is overestimated by a factor of 1.8 as compared with the experimental value<sup>2)</sup> 1388K. The inverse susceptibility follows the Curie-Weiss law though it is considerably upward convex. Calculated effective Bohr magneton numbers at  $T/T_C \sim 1.1$  are obtained to be  $2.4\ \mu_B$  in the static approximation and  $3.0\ \mu_B$  in the 4th-order dynamical CPA. The latter agrees well with the experimental value  $3.2\ \mu_B$ . The amplitude of local moment hardly change with increasing temperatures, and has a value  $2.66\ \mu_B$  around 2600K. This is close to the effective Bohr magneton number 2.55 in the local moment model, but is smaller than the experimental value  $3.2\ \mu_B$ .

Calculated DOS for the ferromagnetic Ni is shown in Fig. 9. By comparing the DOS with those in the static approximation, we find that the dynamical effects reduce the exchange splitting by a factor of two and cause a kink at the Fermi level corresponding to a quasi-particle state. On the other hand, a satellite which is found experimentally around 6 eV below the Fermi level<sup>59–63)</sup> does not appear. It indicates that the dynamical corrections up to the 4th order with asymptotic approximation are not enough to describe the charge fluctuations at low temperatures  $T \lesssim 500\text{K}$ , though the 6 eV satellite is found at  $\omega = -0.45\text{Ry}$  in the DOS when calculated at high temperatures in the paramagnetic state (see the thin dashed curve and thin solid curve in Fig. 9).

The effective potential in Ni shows a single minimum in both the ferro- and the para- magnetic states as shown in Fig. 10, indicating small thermal spin fluctuations around the equilibrium points. The dynamical contribution to the effective potential in the ferromagnetic Ni shows a flat structure with a slope along  $\xi_z$  direction (see Fig. 11);  $E_{\text{dyn}}(\xi) \sim \xi_z h_{\text{eff}}$  where  $h_{\text{eff}}$  is an effective field. This implies that the dynamical effects act as an effective magnetic field which weakens the spin polarization.

The magnetization vs temperature curves are pre-

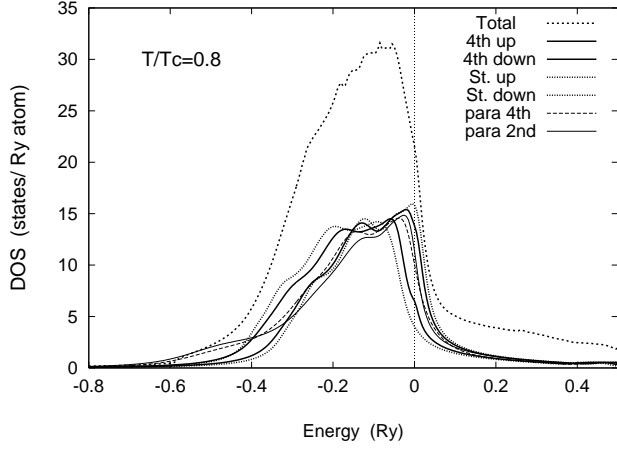


**Fig. 9.** Up and down  $d$  partial DOS of Ni in the static approximation (dotted curves) and in the 4th-order dynamical CPA (solid curves). The total DOS in the 4th-order dynamical CPA is shown by dashed curve. The  $d$  DOS in the paramagnetic state ( $T = 2000\text{K}$ ) are also shown by thin dashed curve (4th-order dynamical CPA) and thin solid curve (2nd-order dynamical CPA).

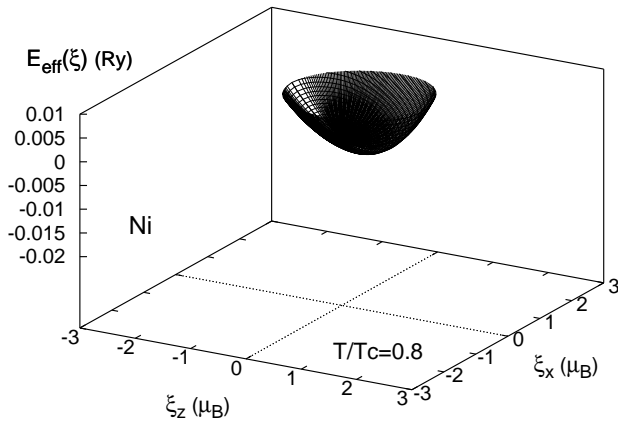


**Fig. 10.** Effective potential of Ni at  $T/T_C = 0.8$ .

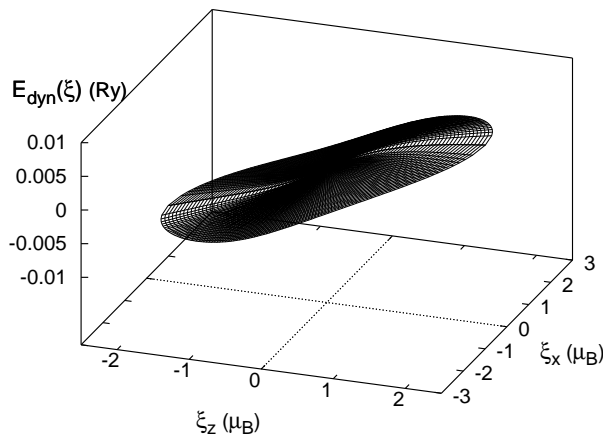


**Fig. 11.** Dynamical contribution to the effective potential in Ni at  $T/T_C = 0.8$ .

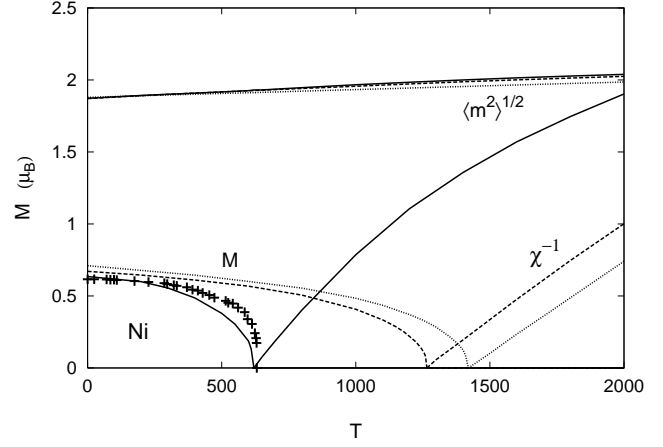


**Fig. 12.** Magnetization vs temperature curves ( $M - T$ ), inverse susceptibilities ( $\chi^{-1}$ ), and the amplitude of local magnetic moments ( $\langle m^2 \rangle^{1/2}$ ) for Ni in the static approximation (dotted curves), the 2nd-order dynamical CPA (dashed curves), and the 4th-order dynamical CPA (solid curves), respectively. Experimental data of magnetization curve<sup>12)</sup> are shown by +.

sented in Fig. 12. We find calculated Curie temperatures: 1420K (static approximation), 1260K (2nd-order dynamical CPA), and 620K (4th-order dynamical CPA), respectively. These results are much lower than the Hartree-Fock value 4940 K. The 4th-order result is in good agreement with the experimental value<sup>3)</sup> 630K. The stability of the ferromagnetism in Ni is sensitive to the change of the DOS at the Fermi level according to the ground-state theory of the ferromagnetism in the low density limit.<sup>29)</sup> A large reduction of  $T_C$  due to 4th-order dynamical corrections seems to be associated with the instability of the ferromagnetism due to the reduction of the DOS at the Fermi level. In fact, the band width of the  $d$  DOS in the 4th-order dynamical CPA is broader than that of the 2nd-order one, and the height of the peak in the 4th order DOS is smaller than the 2nd-order one as shown in Fig. 9.

Calculated inverse susceptibilities in Ni follow the Curie-Weiss law in the static approximation and in the 2nd-order dynamical CPA, but show an upward convexity in the case of the 4th-order dynamical CPA. The upward convexity in the high-temperature region is found in the experimental data,<sup>9)</sup> though it is not the case in Co. Effective Bohr magneton numbers calculated at  $T \sim 2000\text{K}$  are  $1.2 \mu_B$  in the static approximation as well as in the 2nd-order dynamical CPA, while  $1.6 \mu_B$  in the 4th-order dynamical CPA. The latter is in good agreement with the experimental value<sup>9)</sup>  $1.6 \mu_B$ . Calculated amplitude of local moment  $\langle m^2 \rangle^{1/2}$  slightly increases with increasing temperature and takes a value  $1.97 \mu_B$  at 1000K, which is larger than  $1.27 \mu_B$ , the value in the local moment model. Because of the hybridization of the  $d$  bands with the  $sp$  bands, the  $d$  electron number in the metallic state ( $n_d = 8.7$ ) is smaller than  $n_d = 9.4$  expected from a  $d$  band model with the strong ferromagnetism, so that the amplitude of the local magnetic moment is larger than the value expected from the local moment model,  $\sqrt{M(0)(M(0) + 2)}$  where  $M(0)$  denotes



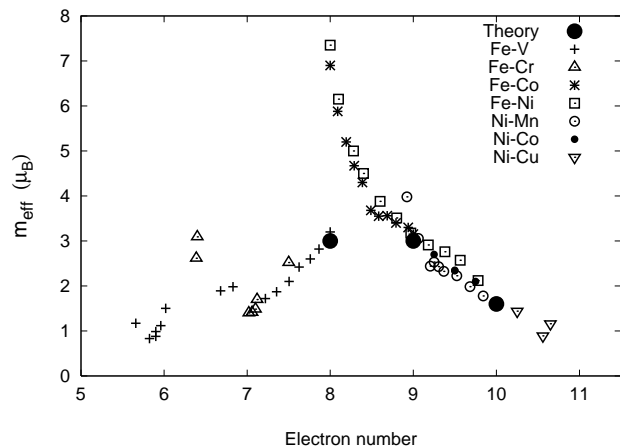


**Fig. 13.** Effective Bohr magneton numbers in various 3d transition metal alloys as a function of conduction electron number per atom.<sup>64–73</sup> Large closed circles show theoretical values of Fe, Co, and Ni obtained in the present calculations.

the ground-state magnetization.

#### 4. Summary and Discussions

We have investigated the ferromagnetic properties of Fe, Co, and Ni on the basis of the first-principles dynamical CPA combined with the LDA +  $U$  Hamiltonian in the TB-LMTO representation. The dynamical CPA takes into account single-site spin and charge fluctuations. We adopted the harmonic approximation to solve the impurity problem in the self-consistent dynamical CPA. In the harmonic approximation, we start from the high temperature approximation, *i.e.*, the static approximation, and take into account individually the dynamical contributions from the dynamical potentials with a given frequency. We have performed the numerical calculations taking into account the dynamical effects up to the 4th order in Coulomb interaction. Calculated effective potential shows up the double minimum structure in case of Fe, the single minimum structure in case of Ni, and the Co is in between the two.

We found that dynamical effects reduce the exchange splitting in the ferromagnetic DOS, suppress the band broadenings due to thermal spin fluctuations in the static approximation, and cause the ‘6 eV’ satellites. In the case of Co and Ni, we also found the quasiparticle peaks at the Fermi level.

We calculated the magnetization vs temperature curves. Curie temperatures obtained from the 4th-order dynamical CPA are 1930K for Fe, 2550K for fcc Co, and 620K for Ni. Although calculated  $T_C$  in Ni is close to the experimental value 630K, those in Fe and Co are overestimated by a factor of 1.8 in comparison with the experimental values, 1040K (Fe) and 1388K (Co), respectively. In the present calculations, the ground state magnetizations obtained by an extrapolation are  $2.58 \mu_B$  (Fe),  $1.82 \mu_B$  (Co), and  $0.63 \mu_B$  (Ni), which are considerably larger than the experimental values,  $2.22 \mu_B$  (Fe),<sup>7)</sup>  $1.74 \mu_B$  (Co),<sup>8)</sup> and  $0.62 \mu_B$  (Ni).<sup>7)</sup> These facts suggest that the present calculations tend to underestimate the screening of Coulomb interactions, especially at low temperatures.

It is desirable to take into account dynamical effects more accurately in order to suppress the magnetization below  $T_C$ . One has also to take into account inter-site spin correlations in order to realize quantitative description of the Curie temperature, going beyond the single-site approximation.

We have calculated the paramagnetic susceptibilities. Calculated effective Bohr magneton numbers,  $3.0 \mu_B$  (Fe),  $3.0 \mu_B$  (Co), and  $1.6 \mu_B$  (Ni), quantitatively explain the experimental data as shown in Fig. 13. Experimental data of effective Bohr magneton numbers in 3d transition metal alloys<sup>64–73</sup> continuously distribute including the three points for Fe, Co, and Ni. It is a future problem to investigate whether or not the dynamical CPA can quantitatively describe these data after extension of the theory to alloys.

#### Acknowledgment

The present work is supported by Grant-in-Aid for Scientific Research (22540395). Numerical calculations have been partly carried out with use of the SGI Altix ICE 8400EX in the Supercomputer Center, Institute of Solid State Physics, University of Tokyo.

- 1) A. Arrott and J.E. Noakes: Phys. Rev. Lett. **19** (1967) 786.
- 2) R.V. Colvin and S. Araj: J. Phys. Chem. Solids **26** (1965) 435.
- 3) J.E. Noakes, N.E. Tornberg and A. Arrott: J. Appl. Phys. **37** (1966) 1264.
- 4) Y. Takehashi: Adv. in Phys. **53** (2004) 497; Phil. Mag. **86** (2006) 2603.
- 5) J. Schäfer, D. Schrupp, Eli Rotenberg, K. Rossnagel, H. Koh, P. Blaha, and R. Claessen: Phys. Rev. Lett. **92** (2004) 097205.
- 6) X.Y. Cui, E.E. Krasovskii, V.N. Strocov, A. Hofmann, J. Schäfer, R. Claessen, and L. Patthey: Phys. Rev. B **81** (2010) 245118.
- 7) H. Danan, A. Herr, and A.J.P. Meyer: J. Appl. Phys. **39** (1968) 669.
- 8) M.J. Besnus, A.J.P. Meyer, and R. Berninger: Phys. Lett. **32** A (1970) 192.
- 9) M. Fallot: J. de Phys. Rad. V (1944) 153.
- 10) H.H. Potter: Proc. Roy. Soc. London **A 146** (1934) 362.
- 11) H.P. Myers and W. Sucksmith: Proc. Roy. Soc. **A 207** (1951) 427.
- 12) P. Weiss and R. Forrer: Ann. Phys. Paris **5** (1926) 153.
- 13) Ya.A. Kraftmakher and T. Yu. Romashina: Soviet Phys. -Solid State **7** (1966) 2040.
- 14) M. Braun and R. Kohlhaas: Z. Naturforsch **19 a** (1964) 663.
- 15) D.L. Connelly, J.S. Loomis, and D.E. Mapother: Phys. Rev. B **3** (1971) 924.
- 16) O. Gunnarson: Physica B **91** (1977) 329.
- 17) J.B. Staunton and B.L. Gyorffy: Phys. Rev. Lett. **69** (1992) 371.
- 18) J. Hubbard: Phys. Rev. B **19** (1979) 2626; **20** (1979) 4584; **23**, (1981) 5974.
- 19) H. Hasegawa: J. Phys. Soc. Jpn. **46** (1979) 1504; **49** (1980) 178.
- 20) R. L. Stratonovich: Dokl. Akad. Nauk. SSSR **115** (1958) 1097 [Sov. Phys. - Dokl. **2** (1958) 416].
- 21) J. Hubbard: Phys. Rev. Lett. **3** (1959) 77.
- 22) W. E. Evenson, J. R. Schrieffer, and S. Q. Wang: J. Appl. Phys. **41** (1970) 1199; J. R. Schrieffer, W. E. Evenson, and S. Q. Wang: J. Phys. (Paris) Colloq. **32** (1971) C1-19.
- 23) G. Morandi, E. Galleani D’Aglia, F. Napoli, and C. F. Ratto: Adv. Phys. **23** (1974) 867.

- 24) M. C. Gutzwiller: Phys. Rev. Lett. **10** (1963) 159.
- 25) M.C. Gutzwiller: Phys. Rev. **134** A (1964) 923.
- 26) M.C. Gutzwiller: Phys. Rev. **137** A (1965) 1726.
- 27) J. Hubbard: Proc. R. Soc. London **A276** (1963) 238.
- 28) J. Hubbard: Proc. Roy. Soc. London **A 281** (1964) 401.
- 29) J. Kanamori: Prog. Theor. Phys. **30** (1963) 275.
- 30) Y. Kakehashi and P. Fulde: Phys. Rev. B **32** (1985) 1595.
- 31) H. Hasegawa: J. Phys. Condensed Matter **1** (1990) 9325.
- 32) G. Stollhoff and P. Fulde: Z. Phys. B **29** (1978) 23; J. Chem. Phys. **73** (1980) 4548.
- 33) Y. Kakehashi: Phys. Rev. B **45** (1992) 7196.
- 34) Y. Kakehashi: Phys. Rev. B **65** (2002) 184420.
- 35) Y. Kakehashi: J. Phys. Soc. Jpn **77** (2008) 094706.
- 36) V.I. Anisimov, A.I. Poteryaev, M.A. Korotin, A.O. Anokhin, and G. Kotliar: J. Phys. Condens. Matter **9** (1997) 7359.
- 37) O.K. Andersen, O. Jepsen, and G. Krier: in *Methods of Electronic Structure Calculations* ed. by V. Kumar, O.K. Andersen, and A. Mookerjee (World Scientific Pub., Singapore, 1994) p. 63.
- 38) Y. Kakehashi, M. Atiqur R. Patoary, and T. Tamashiro: Phys. Rev. B **81** (2010) 245133.
- 39) Y. Kakehashi: Phys. Rev. B **66** (2002) 104428.
- 40) S. Hirooka and M. Shimizu: J. Phys. Soc. Jpn. **43** (1977) 70.
- 41) E. Müller-Hartmann: Z. Phys. B **74** (1989) 507.
- 42) M. Jarrell: Phys. Rev. Lett. **69** (1992) 168; M. Jarrell and H.R. Krishnamurthy: Phys. Rev. B **63** (2001) 125102.
- 43) F.J. Ohkawa: Phys. Rev. B **46** (1992) 9016.
- 44) A. Georges and G. Kotliar: Phys. Rev. B **45** (1992) 6479; A. Georges and W. Krauth: Phys. Rev. B **48** (1993) 7167.
- 45) A. Georges, G. Kotliar, W. Krauth, and M. J. Rozenberg: Rev. Mod. Phys. **68** (1996) 13.
- 46) Y. Kakehashi and P. Fulde: Phys. Rev. B **69** (2004) 045101.
- 47) O. Miura and T. Fujiwara: Phys. Rev. B **77** (2008) 195124.
- 48) A.I. Lichtenstein and M.I. Katsnelson, and G. Kotliar: Phys. Rev. Lett. **87** (2001) 067205.
- 49) V.I. Anisimov, F. Aryasetiawan, and A.I. Lichtenstein: J. Phys. Condens. Matter **9** (1997) 767.
- 50) D.J. Amit and C.M. Bender: Phys. Rev. B **4** (1971) 3115; D.J. Amit and H.J. Keiter: Low Temp. Phys. **11** (1973) 603.
- 51) Dai Xianxi: J. Phys. Condens. Matter. **3** (1991) 4389.
- 52) Y. Kakehashi: J. Phys. Soc. Jpn., **50** (1981) 1505; J. Phys. Soc. Jpn., **50** (1981) 2251.
- 53) S. Kirkpatrick, B. Velický, and H. Ehrenreich: Phys. Rev. B **1** (1970) 3250.
- 54) J. Koringa: J. Phys. Chem. Solids **7** (1958) 252.
- 55) H. Ehrenreich and L. M. Schwarz: Solid State Physics, edited by H. Ehrenreich, F. Seitz, and D. Turnbull (Academic, New York, 1976), Vol. 31, p.150.
- 56) H.J. Vidberg and J.W. Serene: J. Low Temp. Phys. **29** (1977) 179.
- 57) T. Bandyopadhyay and D.D. Sarma: Phys. Rev. B **39** (1989) 3517.
- 58) J.B. Mann: Los Alamos Scientific Laboratory Rep. No. LASL-3690 (1967).
- 59) F.J. Himpsel, J.A. Knapp, and D.E. Eastman: Phys. B **19** (1979) 2919.
- 60) D. E. Eastman, F. J. Himpsel, and J. A. Knapp: Phys. Rev. Lett. **44** (1980) 95.
- 61) W. Eberhardt and E. W. Plummer: Phys. Rev. B **21** (1980) 3245.
- 62) H. Martensson and P.O. Nilsson: Phys. Rev. B **30** (1984) 3047.
- 63) S. Nakamura: Jpn. J. Appl. Phys. **30** (1991) L1705.
- 64) E.P. Wohlfarth: J. Magn. Magn. Mater. **7** (1978) 113.
- 65) S. ARAJS, R.V. Colvin, H. Chessin, and J.M. Peck: J. Appl. Phys. **33** (1962) 1353.
- 66) D.J. Lam, D.O. Van Osterburg, M.V. Nevitt, H.D. Trapp and D.W. Pracht: Phys. Rev. **131** (1963) 1428.
- 67) Y. Nakagawa: J. Phys. Soc. Jpn. **11** (1956) 855.
- 68) Y. Barnier, R. Pauthenet, and L. Néel: Cobalt No. 21 (1963) (Cobalt Information Center).
- 69) Y. Nakagawa: J. Phys. Soc. Jpn. **12** (1957) 700.
- 70) V.I. Chechernikov: Zh. Eksp. Teor. Fiz. **42** (1962) 956 [Sov. Phys. -JETP **15** (1962) 659].
- 71) S. Kaya and M. Nakayama: Proc. Phys. Math Soc. Jpn. **22** (1940) 126.
- 72) J.S. Kouvel: J. Phys. Chem. Solids **16** (1960) 107.
- 73) T.J. Hicks, B. Rainford, J.S. Kouvel, and G.G. Low: Phys. Rev. Lett. **22** (1969) 531.